CHINESE OPTICS LETTERS

Vol. 19, No. 4 | April 2021

Combined studies of surface evolution and crack healing for the suppression of negative factors during CO_2 laser repairing of fused silica

Chao Tan (谭 超)[1,†], Linjie Zhao (赵林杰)[1,†], Mingjun Chen (陈明君)[1*], Jian Cheng (程 健)[1**], Zhaoyang Yin (尹朝阳)[1], Qi Liu (刘 启)[1], Hao Yang (杨 浩)[1], and Wei Liao (廖 威)[2]

[1] State Key Laboratory of Robotics and System, Harbin Institute of Technology, Harbin 150001, China

[2] Research Center of Laser Fusion, China Academy of Engineering Physics, Mianyang 621900, China

*Corresponding author: chenmj@hit.edu.cn

**Corresponding author: cheng.826@hit.edu.cn

Received August 20, 2020 | Accepted October 9, 2020 | Posted Online January 4, 2021

In order to reveal the evolution mechanism of repaired morphology and the material's migration mechanism on the crack surface in the process of CO_2 laser repairing surface damage of fused silica optics, two multi-physics coupling mathematical models with different scales are developed, respectively. The physical problems, such as heat and mass transfer, material phase transition, melt flow, evaporation removal, and crack healing, are analyzed. Studies show that material ablation and the gasification recoil pressure accompanying the material splash are the leading factors in forming the Gaussian crater with a raised rim feature. The use of low-power lasers for a long time can fully melt the material around the crack before healing, which can greatly reduce the size of the residual air layer. Combined with the experimental research, the methods to suppress the negative factors (e.g., raised rim, deposited debris, air bubbles) in the CO_2 laser repairing process are proposed.

Keywords: CO_2 laser repairing; fused silica; crack healing; surface evolution.
DOI: 10.3788/COL202119.041402

1. Introduction

Fused silica optics are widely used in terminal optical components of high-power laser devices due to their excellent optical characteristics and process performance. However, UV laser-induced damage to the surface of fused silica inevitably occurs, and the size of the damage pit increases exponentially in subsequent laser irradiation, which seriously affects the stability of optical components and limits the output flux of large high-power solid-state laser devices[1–3].

Research at home and abroad shows that the non-evaporative repairing method of CO_2 laser local irradiation can greatly suppress the growth of surface damage of fused silica optics[4–6]. It has been successfully applied to high-power laser systems in the field of inertial confinement fusion[7–9]. However, the residual stress[10,11], material modification[12,13], surface deformation[14], optical modulation[15], redeposited debris[16], and air bubbles[17] generated during the actual repairing process are the negative factors that limit the improvement of the mitigation effect. It significantly reduces the damage threshold of the fused silica optics. Therefore, controlling and solving these problems is the key to improving the stability of the CO_2 laser repairing method.

Feit *et al.* first proposed the theoretical models of heat conduction, melt flow, evaporation, and gasification in the CO_2 laser repairing process. He pointed out that the recoil pressure generated by the evaporation of the material and the healing of the crack at the bottom of the damage pit might affect the surface quality of the repaired site[18]. Guss *et al.* have found that the 4.6 μm CO_2 laser could repair deeper cracks at the bottom of the damage pit and reduce the occurrence of ablation. The relationship between the crack size and the formation of bubbles after repairing was preliminary analyzed[19]. Palmier *et al.* used an experimental method to study the melt flow and evaporation removal behaviors of the material around the damage pit under different laser parameters, and the evolution law of repaired surface morphology was obtained[4]. He *et al.* analyzed the physical mechanism during laser polishing of fused silica through numerical simulation, and the influences of surface tension, Marangoni effect, and light pressure on the surface processing quality were revealed[20,21]. Zhang *et al.* used two process plans to repair the damage pits with the lateral dimension of

150–250 μm and explored the bubbles' formation mechanism, as well as the method of controlling bubbles[22].

It can be concluded that the research at this stage is more focused on the experimental studies of the mitigation process improvement and repairing effect evaluation, as well as the calculation and analysis using the single mathematical model. There is no systematic study on the phase transition kinetics of the material, the evolution of surface morphology, and the process of crack healing. However, these are the key to revealing the formation mechanism of the negative factors in the CO_2 laser repair process and seeking methods to suppress these factors.

In this Letter, the physical problems (e.g., heat and mass transfer, material phase transition, melt flow, evaporation removal, crack healing, cooling, and freezing) involved in the process of CO_2 laser repairing surface damage of fused silica optics are analyzed through numerical simulation and experimental methods. In order to reveal the evolution mechanism of repaired morphology and the material migration mechanism on the crack surface, two multi-physics coupling mathematical models with different scales are developed, respectively. The models include the material's behaviors of melt flow and evaporation and consider the internal effects of Marangoni, gravity, capillary force, and gasification recoil pressure. Combined with the experimental research, the methods to suppress the negative factors, such as the raised edge around the repaired site and the formation of bubbles, are proposed.

2. Theory and Model

The schematic diagram of non-evaporative CO_2 laser repairing of fused silica surface damage is shown in Fig. 1. Figure 1(b) is the original damage pit on the surface of the fused silica optics measured by the optical microscope (Nikon ECLIPSE E600). The damage pit has the diameter of about 260 μm and the depth of about 60 μm. Cracks of various sizes are distributed at the bottom of the damage pit. When the CW CO_2 laser acts on the surface, the substrate temperature gradually increases. As the center temperature exceeds the melting point of fused silica, the material at the center of the damage pit gradually melts, forming

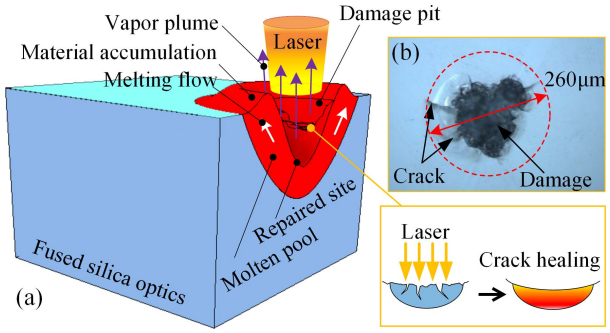

Fig. 1. Schematic diagram of the non-evaporative laser repairing of fused silica surface damage. (a) CO_2 laser repairing schematic; (b) original surface damage pit.

a molten pool. With the increasing of the laser irradiation time, the molten pool gradually expands to the inside of the bulk, and the molten material begins to flow outwards under the action of the Marangoni effect and capillary force. When the substrate temperature exceeds the evaporation temperature, part of the material is evaporated and ablated. At the same time, the gasification recoil pressure formed by the outward splashing of the vapor plume acts on the surface of the molten pool, which prompts a large amount of molten material to flow outwards and gradually accumulate on the edge to form the raised rim. Additionally, the material's melting flow can heal the cracks at the damage pit, and the repaired site with smooth surface morphology is formed eventually. When the laser is off, the substrate temperature decreases instantly, and the molten pool disappears in a short time. The material structure of the repaired site region is modified by the thermal effect of the CO_2 laser.

Since the size range of the micro-cracks around the damage pit is quite different from the scale of the surface damage, the separate models are used to analyze the repairing morphology evolution and crack healing behavior in this work. The thermodynamic and dynamic behaviors of material in the process of CO_2 laser interaction with fused silica can be solved by the conservation equations of mass, momentum, and energy, which can be described as

$$\rho \nabla \boldsymbol{u} = 0, \tag{1}$$

$$\rho C_p \frac{\partial T}{\partial t} + \rho C_p (\boldsymbol{u} \cdot \nabla T) = \nabla \cdot (k \nabla T), \tag{2}$$

$$\rho \frac{\partial \boldsymbol{u}}{\partial t} + \rho(\boldsymbol{u} \cdot \nabla)\boldsymbol{u} = \nabla \cdot [-pA + \mu(\nabla \boldsymbol{u}) + (\nabla \boldsymbol{u})^T] - \rho[1 - \beta(T - T_m)]\boldsymbol{g} + \boldsymbol{F}, \tag{3}$$

where ρ is the density of the material, k is the heat conductivity, C_p is the specific heat capacity, $\boldsymbol{u}$ is the velocity of melting flow, A is the identity matrix, p is the pressure, μ is the dynamic viscosity, T_m is the melting temperature, β is the thermal expansion coefficient, and $\boldsymbol{F}$ is the Darcy damping force.

For material flow in the molten pool, the freely deformable surface is mainly affected by surface tension, in which the thermal capillary force (Marangoni effect) acts in the tangential direction, and its size is related to the temperature gradient. While the capillary force acts in the normal direction, its size is proportional to the curvature of the surface profile. They can be expressed as[20]

$$\sigma = \sigma_0 - \gamma(T - T_m), \tag{4}$$

$$\boldsymbol{\sigma}_n = \kappa \sigma \cdot \boldsymbol{n}, \tag{5}$$

$$\boldsymbol{\sigma}_t = \frac{\partial \sigma}{\partial T} \nabla_s T \cdot \boldsymbol{t}, \tag{6}$$

where σ is the surface tension, σ_0 is the surface tension coefficient, γ is the temperature derivative of surface tension, κ is

the surface curvature, $\nabla_s T$ is the temperature gradient, and $\boldsymbol{\sigma}_n$ and $\boldsymbol{\sigma}_t$ are the normal and tangential components of surface tension, respectively.

When evaporative ablation occurs, part of the laser heat can be taken away by the material escaping outwards, which can be defined as[23]

$$q_{\text{evap}} = M_v \times L_v, \tag{7}$$

where L_v is the latent heat of evaporation, and M_v is the mass flow rate of the escaped vapor plume, which is taken as a function of surface temperature:

$$M_v = \sqrt{\frac{m}{2\pi k_b T}} \times P_{\text{sat}}(T) \times (1 - \beta_r), \tag{8}$$

where m is the atomic mass, and β_r is the retro diffusion coefficient. In this study, taking $\beta_r = 0.17$, P_{sat} is the vapor pressure, which can be expressed as

$$P_{\text{sat}}(T) = P_{\text{atm}} \times \exp\left[\frac{M_a L_v}{R}\left(\frac{1}{T_v} - \frac{1}{T}\right)\right], \tag{9}$$

where R is the ideal gas constant, M_a is the molecular mass, T_v is the evaporation temperature, and P_{atm} is the standard atmospheric pressure. At the same time, the upper surface of the molten pool is subjected to the gasification recoil pressure, which can be defined as

$$P_{\text{recoil}} = \begin{cases} P_{\text{atm}}, & 0 \le T_s < T_v \\ \frac{1+\beta_r}{2} \times P_{\text{sat}}(T_s), & T_s \ge T_v \end{cases}. \tag{10}$$

The mathematical model of this work considers the variations of physical properties of fused silica with respect to temperature, such as thermal conductivity, heat capacity, and dynamic viscosity. The selection of relevant parameters has been published in previous work[23].

3. Results and Discussions

The morphology evolution and phase transition processes under the irradiation of CO_2 lasers with different powers are shown in Fig. 2. The laser used is a 10.6 μm CW laser, with a spatial Gaussian distribution with a spot diameter of 2 mm at $1/e^2$. The laser power is set to 30 W, 31 W, and 32 W in sequence, and the action time is 5 s.

In the heating stage, the material in the molten pool flows outwards under the combined action of Marangoni effect, gravity, and capillary force, of which the Marangoni effect plays a promoting role, while the capillary force acts as an obstacle. When the center material is vaporized and ablated, certain ablation morphology is formed, and the gasification recoil pressure acts on the upper surface of the molten pool. Its value is much greater than the thermal capillary force and capillary force, which prompts the material to flow further to the outside and gradually

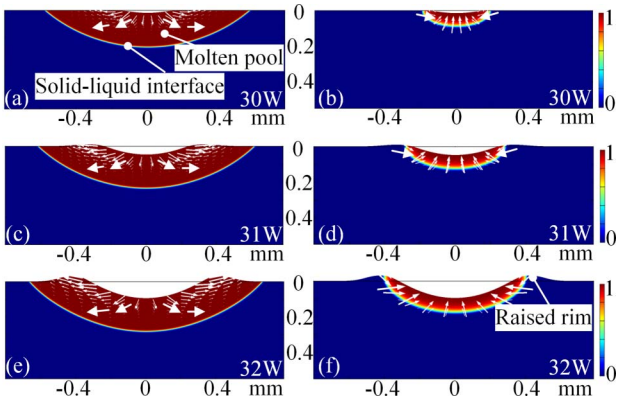

Fig. 2. Surface morphology evolutions and phase transition processes of fused silica optics irradiated by CO_2 lasers with different powers. (a), (c), (e) represent the heating stage at the laser action time of 5 s; (b), (d), (f) are the cases when cooling is for 0.1 s. In the pseudo-color scale, one represents the liquid phase, while zero represents the solid phase.

accumulate at the edge of the molten pool to form the Gaussian crater morphology with raised rim feature, as shown in Figs. 2(a), 2(c), and 2(e). As the laser power increases, the material ablation degree and the gasification recoil pressure increase, and the depth of the Gaussian crater and height of the protrusion become larger and larger. It can be obtained that the gasification recoil pressure is the leading factor in the formation of the Gaussian crater with raised features. When the laser is off, the substrate temperature and the molten pool area temperature decrease rapidly within 0.1 s, as shown in Figs. 2(b), 2(d), and 2(f). The molten material on the raised edge has a tendency to reflow under the action of capillary force; however, it cannot change the final surface morphology because of its small value. It can be seen that the area of the remaining molten pool at the same moment increases as the laser power rises, and the material reflow tendency in this area becomes more obvious. The height of the raised rim has reached 30 μm at the laser power of 32 W, which will cause strong optical modulation and should be strictly controlled.

Figure 3 shows the repaired morphologies obtained by experiments of different laser powers. It is necessary to create a damage pit on the surface of the polished Corning 7980 fused silica glass sample (50 mm length, 50 mm width, 5 mm thickness) before the experiment. The CO_2 laser power used for repairing is 30 W, 31 W, and 32 W, and the laser irradiation time is 5 s. The right side of the experimental morphology in Fig. 3 is the calculated morphology and surface temperature distribution under the same condition.

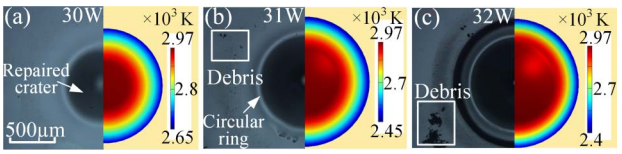

Fig. 3. CO_2 laser repairing experiments of different laser powers and corresponding calculated morphologies under the same condition.

It can be seen from the repaired morphology in Fig. 3 that there are bright circular rings and redeposited debris around the repaired crater, which indicates that material evaporation occurs, and the raised rim feature is formed on the edge in the actual laser repairing process. The greater the laser power, the more severe the material ablation, and the more pronounced the raised rim. It shows that the material's evaporative ablation is the leading factor in the formation of the raised feature, which is consistent with the conclusion obtained from the simulation shown in Fig. 2. Since the redeposited debris distributed around the repaired crater will enhance the absorption of light, reasonable laser power and irradiation time should be selected to avoid material ablation in the actual non-evaporative laser repairing process. On the other hand, certain measures can be taken to eliminate these negative factors, such as use of suction device and large spot passivation[24]. The calculated morphology in Fig. 3 is highly consistent with the experiment, and the diameter of the ablation crater increases as the laser power increases. The highest temperature region corresponds to the experimental morphology. Since part of the laser heat is taken away by the escaped evaporative material, the maximum temperature of the fused silica surface is always kept below the vaporization temperature.

Since there are many various cracks at the bottom of the damage pit, the crack healing process, bubble formation mechanism, and its control method during laser repairing will be analyzed below. The schematic diagram of the crack healing process is shown in Fig. 4(a). The diameter of the laser irradiation area above the crack is 10 μm, and the laser power density is the same as the Gaussian spot with the power of 30 W and the diameter of 2 mm at $1/e^2$. The crack healing time τ and the thickness d of the healing area can be approximated by the following formula[18]:

$$\tau = \eta w/(\pi\sigma), \tag{11}$$

$$d = \frac{2\sqrt{\pi}kT_s}{E}a, \tag{12}$$

where η is the dynamic viscosity, w is the crack width, σ is the surface tension, E is the activation energy, and T_s is the maximum temperature of the material surface.

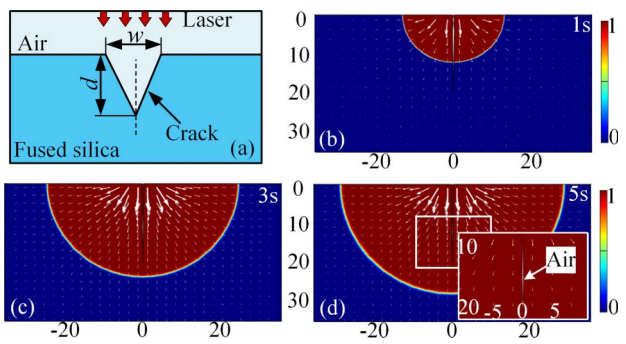

Fig. 4. Evolution process of crack morphology under laser action.

Figures 4(b)–4(d) show the evolution process of crack morphology under the action of the CO_2 laser. Due to the large variation range of the actual crack depth size (from a few microns to hundreds of microns), considering the sizes of the geometric model and the laser spot, the crack depth d is set to 20 μm, and the width w is 0.3 μm. When the CO_2 laser acts on the crack surface, the surface material gradually melts to form a molten pool. The material in the molten pool melts and flows under the effects of Marangoni, capillary force, and gravity, and the top of the crack first closes inwards, as shown in Fig. 4(b). As the laser action time increases, the molten pool gradually expands into the bulk, and the melt flow rate increases. The entire crack is in the liquid phase region at around 3 s, as shown in Fig. 4(c). The crack gradually heals from the top to the bottom until the morphology of the crack surface no longer changes with the increase of laser action time, as shown in Fig. 4(d). From the partially enlarged view of the crack morphology in Fig. 4(d), it can be seen that, although the molten pool continuously expands inwards with the increase of the laser action time, there is always an air interlayer with the length of 10 μm and the width of 0.15 μm at the bottom of the crack. This air layer is due to the fact that, when the CO_2 laser with the power of 30 W equivalently acts on the crack surface, the material at the top of the crack heals first, and the air inside the crack is too late to escape. It corresponds to the formation of bubbles during the actual repairing process. The larger the size of the residual air layer after the crack heals, the larger the bubble formed.

The size of the residual air layer inside the crack irradiated by the laser of different powers is shown in Fig. 5. The action time in the figure is the time from the start of laser irradiation until the crack morphology no longer changes. It can be seen that when the laser power increases from 30 W to 40 W, the width of the air layer increases from 0.15 μm to 0.24 μm, and the length increases from 10 μm to 16 μm. When the laser power is 20 W with the action time of 10 s, the width and length of the air layer after the crack healing are only 0.05 μm and 1 μm. This is because different from the way of crack healing from top to bottom under the

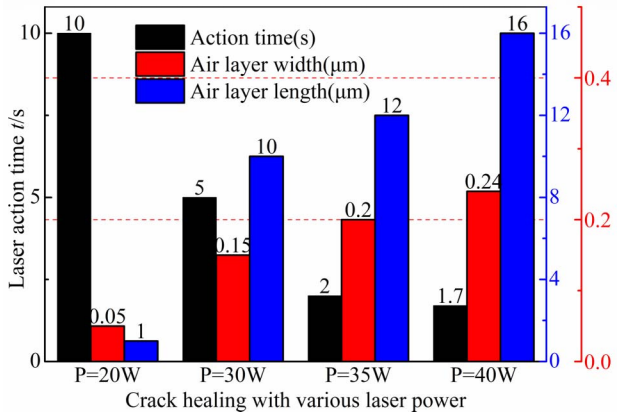

Fig. 5. Size of the residual air layer inside the crack irradiated by the laser of different powers.

action of the high-power laser, the use of a low-power laser for a long time can fully melt the material around the crack before healing, which greatly reduces the size of the residual air layer.

It can be concluded from the above analysis that when the high-power laser is used to repair surface damage directly, it is easy to form large bubbles due to the uneven heating of the material in the damage pit. Therefore, in order to suppress the formation of bubbles, the low-power CO_2 laser is recommended to irradiate the damage pit first for fully preheating the material and prompting the air inside the crack to escape, and then the high-power laser is used to repair it immediately afterwards. The following two different schemes are used to repair the damage pits with the lateral size of about 300 μm and the depth of about 60 μm. In scheme I, the laser power is set to 11 W for 40 s, then 14 W for 20 s, and finally 27 W for 5 s. Scheme II directly uses the laser with power of 27 W for 5 s. The repairing results of the two schemes are shown in Fig. 6.

The mitigation effect with scheme I is better, as shown in Figs. 6(a)–6(c). It can be seen that only one bubble with the diameter of about 9 μm is formed. The bubble of this size will not affect the damage threshold of the fused silica optics. While after repairing with scheme II, a large number of bubbles appear below the repaired surface, as shown in Figs. 6(d)–6(f), most of which are around 10 μm. In the enlarged view, a bubble with the size of 62 μm can be seen. These large numbers of small bubbles are left by many tiny cracks when they are quickly closed at a higher temperature, and the larger-shaped bubbles are formed by deeper cracks. These two types of bubbles should be avoided during the laser repairing process.

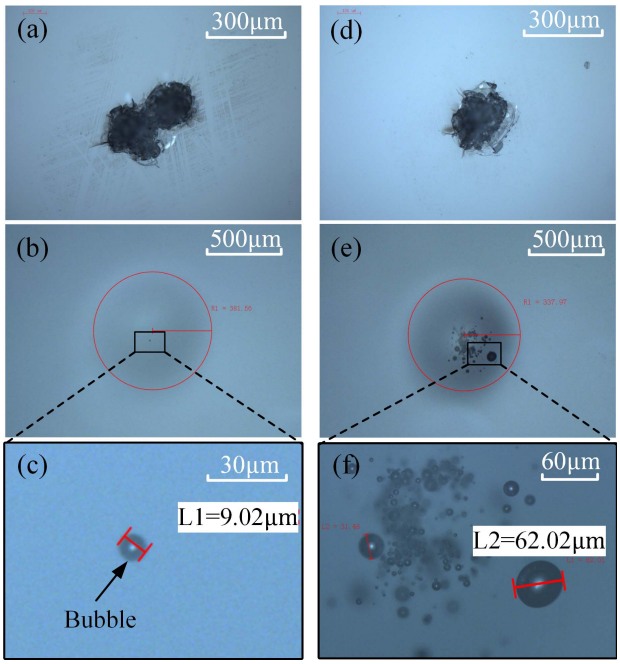

Fig. 6. Repairing results of two processing schemes. (a) and (d) are the initial surface damage morphologies; (b) and (c) are the repairing results of scheme I; (e) and (f) are the repairing results of scheme II.

The presence of bubbles in the CO_2 laser repairing process has a great impact on the ability of resistance to laser damage of fused silica optics. It can be drawn from the experimental test results that the more bubbles and the denser the bubbles, the lower the damage threshold. In order to better control the number of bubbles, it is necessary to optimize the processing parameters during the laser repairing process. The correlations between bubble, crack size, and laser parameters will be further studied in the future.

4. Conclusion

In summary, the physical problems in the process of CO_2 laser repairing surface damage of fused silica optics were studied, including heat and mass transfer, material phase transition, melt flow, evaporation removal, crack healing, cooling, and freezing. The evolution mechanism of repairing morphology and the material migration mechanism of the crack surface were revealed. Studies have shown that material ablation during the laser repairing process and the gasification recoil pressure accompanying the material splashing were the leading factors in forming the Gaussian repaired morphology with raised rim features. The molten material in the cooling stage tended to flow back under the action of capillary force. Furthermore, the use of a low-power laser for a long time can fully melt the material around the crack and prompt the air inside to escape before healing, which could greatly reduce the size of the residual air layer. On the basis of the above research, the methods to suppress the negative factors (e.g., raised rim, deposited debris, and air bubbles) in the CO_2 laser repairing process were proposed.

Acknowledgement

This work was supported by the National Natural Science Foundation of China (Nos. 51775147 and 51705105), Science Challenge Project (No. TZ2016006-0503-01), and Young Elite Scientists Sponsorship Program by CAST (No. 2018QNRC001).

†These authors contributed equally to this work.

References

1. R. A. Negres, G. M. Abdulla, D. A. Cross, Z. M. Liao, and C. W. Carr, "Probability of growth of small damage sites on the exit surface of fused silica optics," Opt. Express **20**, 13030 (2012).
2. R. A. Negres, M. A. Norton, D. A. Cross, and C. W. Carr, "Growth behavior of laser-induced damage on fused silica optics under UV, ns laser irradiation," Opt. Express **18**, 19966 (2010).
3. M. Spaeth, P. Wegner, T. Suratwala, M. Nostrand, J. Bude, A. Conder, J. Folta, J. Heebner, L. Kegelmeyer, and B. MacGowan, "Optics recycle loop strategy for NIF operations above UV laser-induced damage threshold," Fusion Sci. Technol. **69**, 265 (2016).
4. S. Palmier, L. Gallais, M. Commandré, P. Cormont, R. Courchinoux, L. Lamaignère, J. L. Rullier, and P. Legros, "Optimization of a laser mitigation process in damaged fused silica," Appl. Surf. Sci. **255**, 5532 (2009).
5. P. Cormont, P. Combis, L. Gallais, C. Hecquet, L. Lamaignère, and J. L. Rullier, "Removal of scratches on fused silica optics by using a CO_2 laser," Opt. Express **21**, 28272 (2013).

6. Y. Jiang, S. He, W. Liao, C. Yao, H. Wang, B. Wang, S. Guan, R. Qiu, D. Guo, and X. Xiang, "Theoretical and experimental investigations of localized CO_2 laser-fused silica interactions and thermo-mechanical properties of mitigated sites," J. Non-Cryst. Solids **515**, 1 (2019).
7. M. J. Matthews, S. T. Yang, N. Shen, S. Elhadj, R. N. Raman, G. Guss, I. L. Bass, M. C. Nostrand, and P. J. Wegner, "Micro-shaping, polishing, and damage repair of fused silica surfaces using focused infrared laser beams," Adv. Eng. Mater. **17**, 247 (2015).
8. T. Doualle, L. Gallais, S. Monneret, S. Bouillet, A. Bourgeade, C. Ameil, L. Lamaignère, and P. Cormont, "Development of a laser damage growth mitigation process, based on CO_2 laser micro processing, for the Laser MegaJoule fused silica optics," Proc. SPIE **10014**, 1001407 (2016).
9. W. Zheng, X. Wei, Q. Zhu, F. Jing, D. Hu, J. Su, K. Zheng, X. Yuan, H. Zhou, and W. Dai, "Laser performance of the SG-III laser facility," High Power Laser Sci. Eng. **4**, e21 (2016).
10. T. Doualle, A. Ollé, P. Cormont, S. Monneret, and L. Gallais, "Laser-induced birefringence measurements by quantitative polarized-phase microscopy," Opt. Lett. **42**, 1616 (2017).
11. A. Nakamura, T. Mizuta, Y. Shimotsuma, M. Sakakura, T. Otobe, M. Shimizu, and K. Miura, "Picosecond burst pulse machining with temporal energy modulation [Invited]," Chin. Opt. Lett. **18**, 123801 (2020).
12. C. C. Zhang, W. Liao, K. Yang, T. X. Liu, Y. Bai, L. J. Zhang, X. L. Jiang, J. Chen, Y. L. Jiang, H. J. Wang, X. Y. Luan, H. Zhou, X. D. Yuan, and W. G. Zheng, "Fabrication of concave microlens arrays by local fictive temperature modification of fused silica," Opt. Lett. **42**, 1093 (2017).
13. C. Zhang, L. Zhang, X. Jiang, B. Jia, W. Liao, R. Dai, J. Chen, X. Yuan, and X. Jiang, "Influence of pulse length on heat affected zones of evaporatively-mitigated damages of fused silica optics by CO_2 laser," Opt. Lasers Eng. **125**, 105857 (2020).
14. S. Elhadj, M. J. Matthews, and S. T. Yang, "Combined infrared thermal imaging and laser heating for the study of materials thermophysical and processing properties at high temperatures," Crit. Rev. Solid State Mat. Sci. **39**, 175 (2014).
15. C. Tan, L. Zhao, M. Chen, J. Cheng, Z. Yin, Q. Liu, H. Yang, and W. Liao, "Optical modulation of repaired damage site on fused silica produced by CO_2 laser rapid ablation mitigation," Chin. Phys. B **29**, 054209 (2020).
16. L. Gallais, P. Cormont, and J.-L. Rullier, "Investigation of stress induced by CO_2 laser processing of fused silica optics for laser damage growth mitigation," Opt. Express **17**, 23488 (2009).
17. R. M. Brusasco, B. Penetrante, J. A. Butler, and L. W. Hrubesh, "Localized CO_2 laser treatment for mitigation of 351-nm damage growth in fused silica," Proc. SPIE **4679**, 40 (2002).
18. M. D. Feit and A. M. Rubenchik," Mechanisms of CO_2 laser mitigation of laser damage growth in fused silica," Proc. SPIE **4932**, 91 (2004).
19. G. Guss, I. Bass, V. Draggoo, R. Hackel, S. Payne, M. Lancaster, and P. Mak, "Mitigation of growth of laser initiated surface damage in fused silica using a 4.6-micron wavelength laser," Proc. SPIE **6403**, 64030M (2007).
20. T. He, C. Wei, Z. Jiang, Y. Zhao, and J. Shao, "Super-smooth surface demonstration and the physical mechanism of CO_2 laser polishing of fused silica," Opt. Lett. **43**, 5777 (2018).
21. T. He, C. Wei, Z. Jiang, Z. Yu, Z. Cao, and J. Shao, "Numerical model and experimental demonstration of high precision ablation of pulse CO_2 laser," Chin. Opt. Lett. **16**, 041401 (2018).
22. L. J. Zhang, C. C. Zhang, J. Chen, Y. Bai, Y. L. Jiang, X. L. Jiang, H. J. Wang, X. Y. Luan, X. D. Yuan, and W. Liao, "Formation and control of bubbles during the mitigation of laser-induced damage on fused silica surface," Acta Phys. Sin. **67**, 016103 (2018).
23. C. Tan, L. Zhao, M. Chen, J. Cheng, and W. Liao, "Experimental and theoretical investigation of localized CO_2 laser interaction with fused silica during the process of surface damage mitigation," Results Phys. **16**, 102936 (2020).
24. I. L. Bass, G. M. Guss, M. J. Nostrand, and P. J. Wegner, "An improved method of mitigating laser-induced surface damage growth in fused silica using a rastered, pulsed CO_2 laser," Proc. SPIE **7842**, 784220 (2010).